Thermal Behavior of Doubly-Fed Induction Generator Wind Turbine System during Balanced Grid Fault

Zhou, Dao; Blaabjerg, Frede; Lau, Mogens; Tonnes, Michael

Published in:
Proceedings of the 29th Annual IEEE Applied Power Electronics Conference and Exposition, APEC 2014.

DOI (link to publication from Publisher):
10.1109/APEC.2014.6803744

Publication date:
2014

Thermal Behavior of Doubly-Fed Induction Generator Wind Turbine System during Balanced Grid Fault

Dao Zhou, Frede Blaabjerg
Department of Energy Technology
Aalborg University
Aalborg, Denmark
zda@et.aau.dk, fbl@et.aau.dk

Mogens Lau, Michael Tonnes
Danfoss Silicon Power GmbH
Flensburg, Germany
mogens.lau@danfoss.com, michael.tonnes@danfoss.com

Abstract— Ride-through capabilities of the doubly-fed induction generator (DFIG) during grid fault have been studied a lot. However, the thermal performance of the power device during this transient period is seldom investigated. In this paper, the dynamic model for the DFIG and the influence of the rotor current to the damping time of the stator flux and rotor terminal voltage during the symmetrical grid fault is firstly evaluated. Then, the theoretical analysis for the safety operation area of the power device is given in terms of the various voltage dips and various rotor speeds, in which simulation results are used to verify. Finally, the power loss and the thermal profile are shown at the transient period of the DFIG. It is concluded that, in order to guarantee the same damping time of the stator flux, the serious voltage dip results in the higher power losses as well as the junction temperature fluctuation, and may even damage the rotor converter, if the design is not considered carefully.

I. Introduction

The penetration of wind power is expected to achieve 20% of the total electricity production by 2020 in Europe [1]. Because of the noise emission, footprint limitation and richer wind energy, the wind turbines are moving from onshore to offshore. Meanwhile, the lifetime of the wind turbine system are inversely prolonged to 20-25 years under such uncertain and harsh environment, whose mission profile leads to a faster fatigue and might give a higher failure rate. As the most vulnerable power electronic component, more and more efforts have been recently devoted to the reliable behavior of the power semiconductor due to the increased cost and time for repair after failures [2]-[5]. It is widely accepted that the thermal profile of the power semiconductor is an important indicator of the lifetime and it has an influence on the reliable operation. The power cycle number to failure is quite relevant to the junction temperature fluctuation as well as the mean junction temperature [6]-[10].

The Doubly-Fed Induction Generator (DFIG) is a widely used configuration for wind turbines above 1 MW. It provides the advantage of variable speed operation and four-quadrant active and reactive power capabilities using the converter rated for only a small fraction (20%-30%) of the rated power. However, on detecting a grid fault, the generator unit is usually disconnected to protect the vulnerable rotor converter. In the recent years, this has been achieved by so-called crowbar. As the penetration of wind power continues to increase, more wind turbines are required to ride through the grid faults, and to contribute to the system stability after the fault clearance. Researchers are addressing this issue from several points of view. For instance, the study described in [11], [12] analyzes the intrinsic in the DFIG during the grid fault and proposes its dynamic model. Many control strategies are suggested to support the DFIG to ride through the grid fault without the crowbar or with the enable time of the crowbar as soon as possible [13]-[17]. The thermal behavior of the power devices during grid fault is evaluated for both the permanent magnet synchronous generator based full-scale power converter and the DFIG based partial-scale power converter at steady-state operation [18], [19].

This paper focuses on the transient thermal behavior of the DFIG wind turbine system during the balanced grid fault, in order to identify critical issues which can cause lifetime reduction. Section II is a brief introduction to the dynamics of the DFIG model, and then the influence of rotor current on the stator flux damping and the rotor terminal voltage is analyzed in section III. The safety operation area of the traditional demagnetizing control is theoretically studied and verified by the simulation in section IV. The power loss and thermal profile of the switching power device is shown in Section V. Finally, conclusions are drawn in the last section.

II. Dynamic DFIG Model under Grid Fault

A lot of references have discussed the modeling of DFIG under grid faults [11]-[17]. If the stator reference frame, static to the stator winding, is introduced, assuming the rotor variables are all transferred to the stator-side, the voltage equation of the generator's stator and rotor can be expressed as follows,

$$\boldsymbol{u}_s = R_s \boldsymbol{i}_s + \frac{d}{dt}\boldsymbol{\psi}_s \tag{1}$$

$$\boldsymbol{u}_r = R_r \boldsymbol{i}_r + \frac{d}{dt}\boldsymbol{\psi}_r - j\omega_m \boldsymbol{\psi}_r \tag{2}$$

where $\boldsymbol{u}$, $\boldsymbol{i}$ and $\boldsymbol{\psi}$ are the space vector of voltage, current and flux of the induction generator, respectively. R denotes the generator's intrinsic resistance, and ω_m denotes the rotor angular frequency. The subscripts s and r denote stator quantities and rotor quantities. The additional third term in (2)

represents the compensation transforming from the rotor reference frame to the stator reference frame, where the rotor reference frame rotates correspondingly at rotor speed with respect to the stator winding.

Similarly, with the aid of the stator reference frame, the stator flux $\boldsymbol{\psi}_s$ and rotor flux $\boldsymbol{\psi}_r$ equations are given by,

$$\boldsymbol{\psi}_s = L_s \boldsymbol{i}_s + L_m \boldsymbol{i}_r \tag{3}$$

$$\boldsymbol{\psi}_r = L_m \boldsymbol{i}_s + L_r \boldsymbol{i}_r \tag{4}$$

where L_m is the magnetizing inductance, and L is the self-inductance of stator-side and the rotor-side of the DFIG.

In normal operation, the space vector of stator flux rotates at slip speed ω_r with respect to the rotor winding, which is the product of the slip s and the synchronous angular speed ω_s. However, during a balanced full-dip grid voltage fault, the dc component of the stator flux appears, and the stator flux no longer rotates but freezes with the respect to the stator winding. As a result, the stator flux is rotating at speed ω_m with respect to rotor winding. In the case of a balanced partial-dip grid voltage fault, the stator flux can consequently be expressed as a sum of a forced flux $\boldsymbol{\psi}_{sf}$ and a natural flux $\boldsymbol{\psi}_{sn}$ [7],

$$\boldsymbol{\psi}_s = \boldsymbol{\psi}_{sf} + \boldsymbol{\psi}_{sn} \tag{5}$$

According to the superposition principle, the dynamic model of the DFIG is thus depicted in terms of two independent circuits: the forced machine model and the natural machine model. For the forced machine shown in Fig. 1(a), it stands for the steady-state operation of the DFIG, where the stator of the induction generator connects to the remaining grid voltage (p is the voltage dip level), and no transient stator flux is considered. On the other hand, the natural machine shown in Fig. 1(b) is used for a transient period, whose stator is short-circuited, and an initial natural flux exists in the stator. In order to investigate the dynamic response of the DFIG under grid fault, only the natural machine is focused in the following.

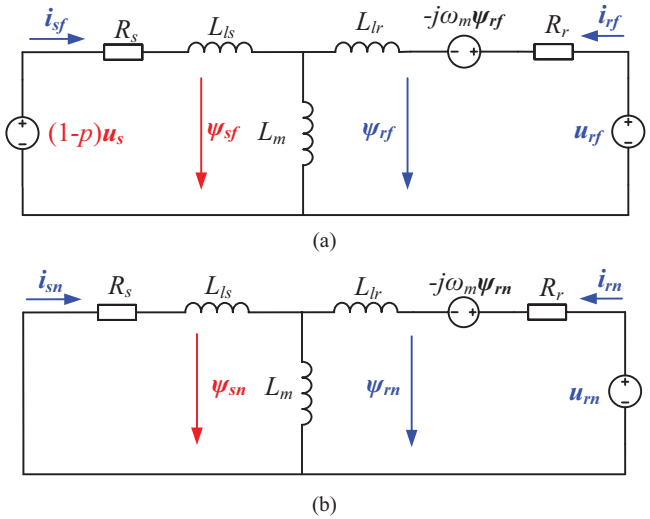

Fig. 1. Dynamic model of the DFIG under a balanced grid fault. (a) Forced machine model; (b) Natural machine model.

III. Influence of Rotor Current Under DFIG Natural Model

DFIG based wind turbine generators shown in Fig. 2 are susceptible to grid-side low voltage or short-circuit due to the presence of the power electronics converter on the rotor-side. If a three-phase voltage sag happens on the grid-side, as aforementioned, a dc component of stator natural flux emerges immediately, which induces a considerably increase of electromagnetic force (EMF). The rotor current thus increases substantially without proper protection, and may even damage the rotor converter. Moreover, the existence of stator natural flux prevents the rotor converter to provide the reactive power injection. As a consequence, the damping time of the stator flux and analysis of rotor voltage are two important aspects in case of grid faults. However, in normal operation, the rotor converter is designed to adjust the active power and the reactive power of the stator side through the controllability of the rotor current. This section will investigate the effect of the rotor current on DFIG's natural flux evolution and induced rotor voltage.

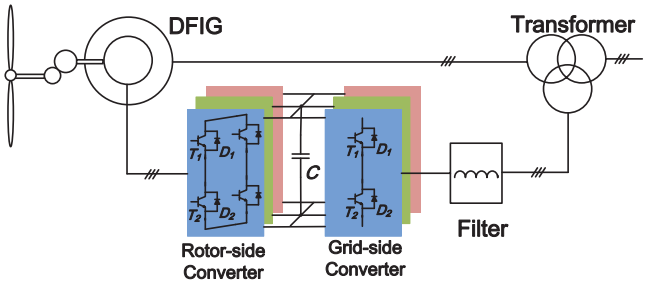

Fig. 2. Configuration of the wind turbine system equipped with DFIG.

A. Natural flux evolution

According to Fig. 1(b), as no stator voltage in the natural machine model is taken into account, expressing the relationship between the stator flux and the rotor current through (1) and (3) yields,

$$\frac{d}{dt}\boldsymbol{\psi}_{sn} = -\frac{R_s}{L_s}\boldsymbol{\psi}_{sn} + \frac{R_s}{L_s}L_m \boldsymbol{i}_{rn} \tag{6}$$

where the subscript n indicates the variables in natural machine model. If the rotor side is open-circuit, from the first term, it is inferred that the natural flux is exponentially decaying with the DFIG's own time constant, whose value is quite large, up to 1 to 1.5 seconds for a MW generator [12]. If no counter-action is adopted, the transient period remains for several seconds, which is unfortunately a violation with the fast response of the reactive power defined in the recent grid codes [20], [21].

The second term denotes the influence of rotor current in the evolution of the stator flux. Depending on the phase angle between the rotor current and the natural flux, the damping could be either accelerated or decelerated. For instance, if the rotor converter injects a current in phase with the natural flux, the damping of the stator flux will be slowed down, and might even be canceled out or become negative. Under this

specific situation, the natural flux will not disappear, but rather increase until the rotor converter goes out of control.

The opposite situation happens if a crowbar is connected to the rotor. The crowbar is a protection against the grid faults that allows a low resistance across the rotor windings. The connection of the crowbar generates the circulation of large current through the rotor windings and stator windings. Since the rotor current is almost in opposite phase to the natural flux, the flux damping will be accelerated. However, this hardware solution is hardly helpful in injecting reactive power, and inevitably increases the cost of the system.

B. Voltage at rotor terminals

Based on (3) and (4), the rotor flux can be represented in terms of the stator flux and rotor current by eliminating the stator current. If the rotor reference frame is introduced, the previous expression of the rotor voltage in (2) can be transformed as the following,

$$\boldsymbol{u}_{rn}^{r} = (R_r + \sigma L_r \frac{d}{dt})\boldsymbol{i}_{rn}^{r} + \frac{L_m}{L_s}\frac{d}{dt}\boldsymbol{\psi}_{sn}^{r} \tag{7}$$

where the superscript r denotes the rotor reference frame, and σ denotes the leakage inductance coefficient $\sigma=1-L_m^2/L_sL_r$. It is observed that the first term of the expression is the voltage drop in the rotor resistance and in the transitory rotor inductance, and the second term of the expression is the EMF induced by the stator flux in rotor windings. If (6) is deduced under the rotor reference frame, (7) can be further simplified as [22],

$$\boldsymbol{u}_{rn}^{r} \approx (R_r + R_s)\boldsymbol{i}_{rn}^{r} - j\sigma\omega_m L_r \boldsymbol{i}_{rn}^{r} - j\omega_m \boldsymbol{\psi}_{sn}^{r} \tag{8}$$

Viewed from the rotor, the DFIG behaves as EMF $\boldsymbol{e}_{rn}$ induced by the stator natural flux, in series with rotor and stator resistance as well as the transitory inductance of the machine. The equivalent circuit of the machine is thus depicted in Fig. 3. In order to guarantee the current controllability, the rotor converter should be sized to generate a voltage at least larger than the EMF.

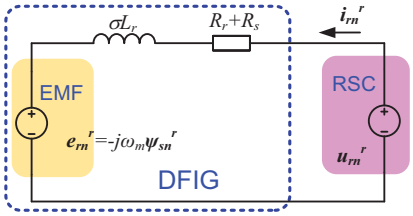

Fig. 3. Equivalent machine model in viewpoint of the rotor.

IV. Control for Grid Fault Ride-through Operation

Xiang *et. al* [11] proposed the demagnetizing control technique to protect the rotor converter against the grid faults without a crowbar or with a crowbar active time as short as possible [12]. In this section, the demagnetizing control scheme will briefly be described. Then the Safety Operation Area (SOA) will be theoretically analyzed in terms of various voltage dip levels and various rotor speeds. After that, the SOA is verified by simulation results.

A. Demagnetizing current influence to stator flux

The basic idea of the demagnetizing current is to introduce a rotor current opposite to the stator flux,

$$\boldsymbol{i}_{rn} = -k\boldsymbol{\psi}_{sn} \tag{9}$$

Substituting (9) into (6), the evolution of the stator flux is then obtained,

$$\frac{d}{dt}\boldsymbol{\psi}_{sn} = -(\frac{R_s}{L_s} + \frac{R_s}{L_s}L_m k)\boldsymbol{\psi}_{sn} \tag{10}$$

The stator flux is exponentially decaying with the certain time constant,

$$\tau_s = \frac{L_s}{R_s(1+kL_m)} \tag{11}$$

It shows that the introduction of the demagnetizing current will accelerate the decaying of the natural flux.

B. Demagnetizing current effects on rotor voltage

Consider that the generator operates under normal operation until a symmetrical voltage dip occurs at a given moment $t=0$. The space vector of the grid voltage is,

$$\boldsymbol{u}_s = \begin{cases} U_s e^{j\omega_s t} & t \le 0 \\ (1-p)U_s e^{j\omega_s t} & t > 0 \end{cases} \tag{12}$$

where U_s denotes the amplitude of the grid voltage.

Neglecting the insignificant voltage drop through the stator resistance, the stator flux after the grid fault can be obtained,

$$\boldsymbol{\psi}_s = -j(\frac{(1-p)U_s}{\omega_s}e^{j\omega_s t} + \frac{pU_s}{\omega_s}e^{-\frac{t}{\tau_s}}) \tag{13}$$

The first term can be regarded as stator forced flux $\boldsymbol{\psi}_{sf}$, still rotating with synchronous angular speed. The second term is the stator natural flux $\boldsymbol{\psi}_{sn}$, static with stator winding. The amplitudes of these two kinds of stator flux are dictated by the voltage dip level.

Assuming the grid voltage is the reference vector, Fig. 4 graphically shows the space vector diagram of the rotor voltage. The stator flux $\boldsymbol{\psi}_{sn}$ is lagging the stator voltage $\boldsymbol{u}_s$ 90 degree, and the rotor current $\boldsymbol{i}_{rn}$ is opposite to the stator flux.

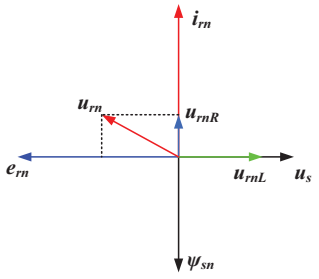

Fig. 4. Space vector diagram for rotor voltage under stator reference frame.

According to (8), the voltage drop $\boldsymbol{u}_{rnR}$ through the resistance and $\boldsymbol{u}_{rnL}$ transitory inductance is in phase of rotor current and lagging the current 90 degree, respectively.

Moreover, the EMF e_{rn} is lagging the stator flux 90 degree. It is noted that, besides the acceleration of damping stator flux, the demagnetizing control normally has an advantage to reduce the rotor voltage as well.

C. Analysis of safety operation area

The rotor converter usually employs the IGBT module as a semiconductor switching device. Its continuous current rating is determined by the steady-state current, while during the transient period the over-current may occur. Generally speaking, the maximum current switched by the power device can be the peak pulse rating, as long as the junction temperature is still permissible and the *V-I* switching trajectory is within the SOA. The pulse current rating of an IGBT module is typically two times of the continuous current rating. As mentioned before, the stator natural flux induces the overcurrent and overvoltage in the rotor converter during a balanced grid fault. From (8) and (13), the EMF is jointly decided by the voltage dip level and rotor speed. Therefore, it is interesting to investigate the SOA of the rotor converter in terms of various voltage dip levels and various rotor speeds, in which the instantaneous rotor current is constrained below 2.0 pu., while the rotor converter dc-link voltage is also maintained below the device voltage rating.

A 2 MW DFIG wind turbine is used for the case study, whose parameters are given in Appendix. Because of a low-voltage system, a common 1 kA/1.7 kV power module from leading manufacturer is selected. Based on (8), the relationship between the rotor voltage and the rotor current at different voltage dips is shown in Fig. 5, in which the rotor speed is set at 1800 rpm. It can be seen that, if the rotor is open-circuit, the higher dip level causes the higher EMF viewed from rotor side. Besides, the demagnetizing current reduces the rotor voltage, and even brings the rotor converter back to SOA with a proper amount of the demagnetizing current. Due to partial-scale feature compared to the generator, the rotor converter will be destroyed by serious voltage dip, e.g. when the dip level reaches 0.8 pu.

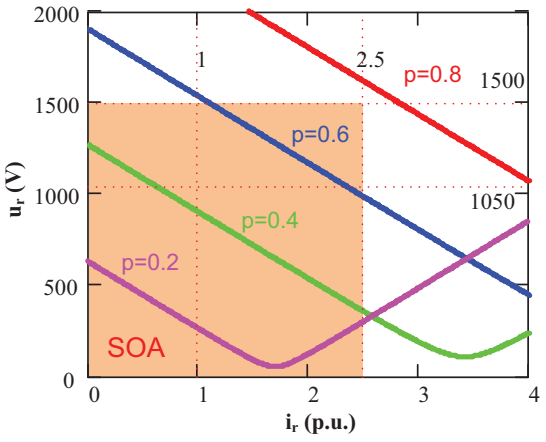

Fig. 5. Voltage amplitude at rotor terminal versus rotor current with various grid voltage dips at rotor speed 1800 rpm, where p is the voltage dip.

During the grid fault, the demagnetizing current injection results in an even higher rotor speed [11]. The rotor speed is assumed to be 1950 rpm in comparison with the maximum normal speed 1800 rpm. Fig. 6 shows the relationship between the rotor voltage and the rotor current at different rotor speeds when the voltage dip is 0.8 pu. It is noted that the higher rotor speed also induces higher EMF of the rotor, and the rotor converter is able to ride through the grid fault easier at lower rotor speed.

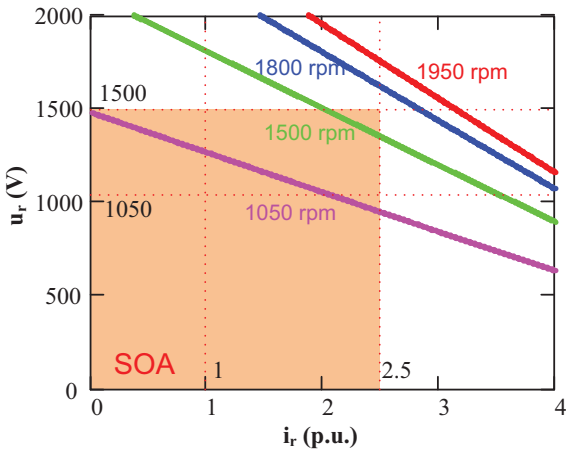

Fig. 6. Voltage amplitude at rotor terminal versus rotor current with various rotor speeds at the voltage dip: p=0.8.

D. Simulation validation

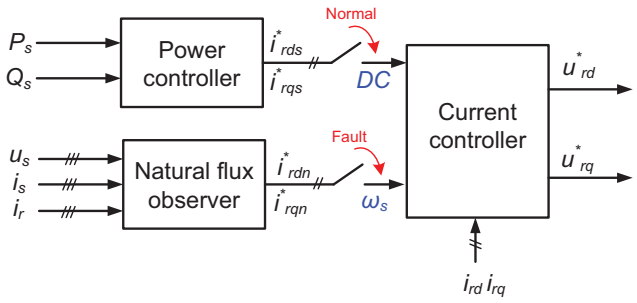

Fig. 7. Control diagram for rotor converter during normal operation and grid fault condition.

The control scheme for the rotor converter is shown in Fig. 7, where the control objective is switched from the active power and the reactive power to the demagnetization of the stator transient flux if the grid fault happens. The rotor reference current is obtained through a natural flux observer, due to its dc component viewed from the stator-side, the rotor reference current becomes a grid angular frequency ω_s viewed from the rotor side. However, in normal operation, the rotor reference current is a dc component viewed from the rotor side. As a result, the actual frequency of the rotor current in the case of the grid fault is the rotor speed, while in normal operation the frequency of the rotor current becomes the slip speed.

The wind turbine is required to start injecting reactive power in about 500 ms to 600 ms from the beginning of the fault, complying with the latest grid code requirement [20], [21]. The damping time for the stator flux is consequently set at 180 ms. As shown in Fig. 8, the stator flux returns to normal within around 600 ms, which is consistent with the above

damping time design. Furthermore, the stator current may reach up to 3 pu, and it has two frequencies during the transient period: the dc component and the grid frequency as illustrated in (13).

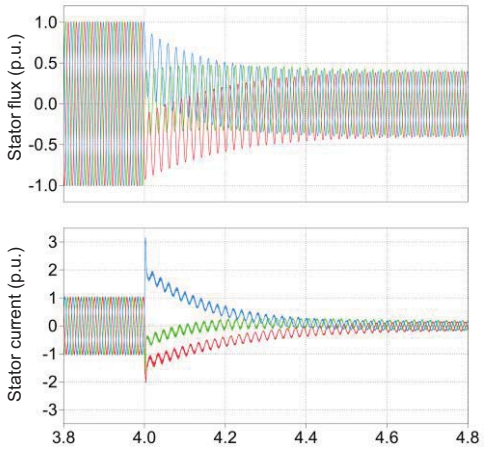

Fig. 8. Damping time of natural flux (e. g. rotor speed at 1800 rpm and voltage dip at 0.6).

The rotor voltage and the rotor current are then shown in Fig. 9 with the different voltage dip levels. In order to verify the evaluation in Fig. 5, four various dip levels are independently simulated. In Fig. 9(a) and Fig. 9(b), the rotor converter can survive through the grid fault. In Fig. 9(d), as the rotor voltage is higher than 1500 V, it excesses the linear modulation index and the rotor converter loses the control of the rotor current. The above phenomena agree with the analysis in Fig. 5. However, in Fig. 9(c), in case of the voltage dip at 0.6 pu, the simulation shows that the rotor side converter operates out of the SOA during the fault ride-through period. It is due to the error introduced by the control gain.

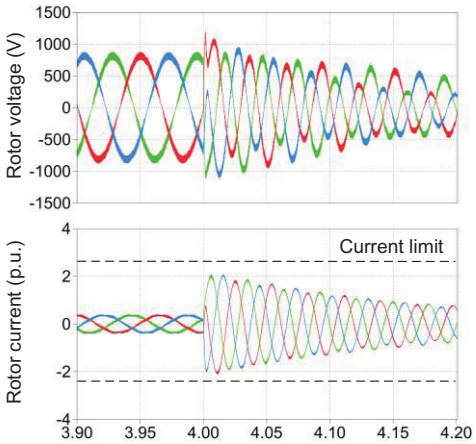

Fig. 10. Simulation of SOA vs. rotor speed in case of dip level at 0.8 and rotor speed at 1050 rpm.

Fig. 10 shows the simulation of SOA versus rotor speed in the case of the voltage dip at 0.8 pu, and the rotor speed at 1050 rpm. Compared with the simulation in Fig. 9(d), it is obvious that if the rotor speed is reduced, it is possible for the rotor converter to ride through the same serious voltage dip.

V. Thermal Behavior of Power Device

As the demagnetizing control introduces the various rotor current as well as the rotor voltage at different voltage dips and rotor speeds, this section will analyze the power loss distribution and the thermal cycling of power device in the case of a balanced grid fault.

A. Power loss distribution

The power loss model, consisting of the conduction losses and switching losses, can be referred to [23], [24]. Based on the on-state voltage drop and switching energy against the load current and the DC-link voltage provided by the manufacturers, the conduction losses and switching losses are accumulated by every switching cycle within one fundamental frequency. The simulation of the power loss has been obtained with the use of PLECS blockset in Simulink [25].

According to Fig. 9, it is noted that the current of the rotor in the three phases becomes extremely unbalanced. Moreover, as the current is exponential decaying, the maximum current through the power modules in the upper and lower of the same bridge is also different. Fig. 11 shows power loss distribution of the most stressed power device at different grid voltage dips, and Fig. 11(a) and Fig. 11(b) are the situations for the rotor speed at 1800 rpm and 1050 rpm, respectively.

In the case of the rotor speed at 1800 rpm from Fig. 11(a), during the normal operation, it is noted that the conduction loss are mainly consumed by the diode compared to the IGBT because of its power flow direction in the super-synchronous mode. However, it is the IGBT that dissipates higher switching loss due to the fact that the turn-on and turn-off energy in the IGBT has larger value than the reverse recovery energy in the diode according to the manufacturer's datasheet. With the increase of the voltage dip level, the natural stator flux becomes higher. In order to guarantee the same damping time of the stator flux, the initial rotor current becomes higher, which causes the increasing power loss.

In the case of the rotor speed at 1050 rpm from Fig. 11(b), due to the maximum power point tracking, the generated power is much lower than the rotor speed at 1800 rpm in the normal operation. Therefore, the power devices are considerably less stressed. Moreover, in the sub-synchronous mode, the direction of the active power through the rotor converter is also reverse, which implies that the IGBT consumes higher conduction loss. Similarly, the more serious voltage dip, the heavier the power device is loading. Furthermore, at the same grid dip 0.8, the power loss at rotor speed 1800 rpm is higher than the case at 1050 rpm, which agrees with the rotor current and voltage characteristic shown in Fig. 9(d) and Fig. 10.

B. Thermal cycling

The thermal model of the power devices, including the IGBT and the freewheeling diode are shown in Fig. 12 in the form of the power module, the thermal grease and the heat-sink. The electrical analogies representing thermal variables are used, in which the power dissipation in the IGBT and the

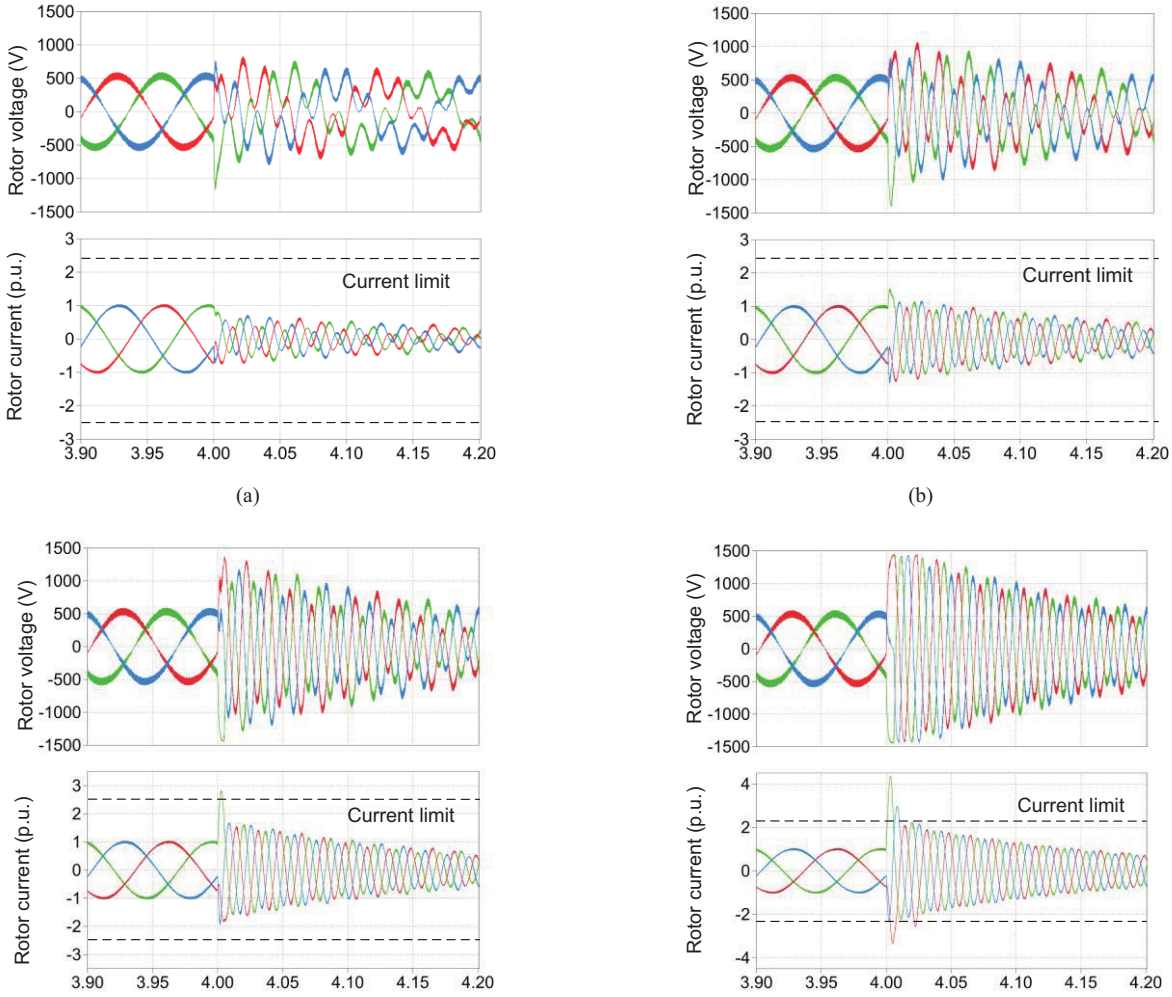

Fig. 9. Simulation of safety operation area vs. dip level in case of rotor speed=1800 rpm at different voltage dips. (a) p=0.2; (b) p=0.4; (c) p=0.6; (d) p=0.8.

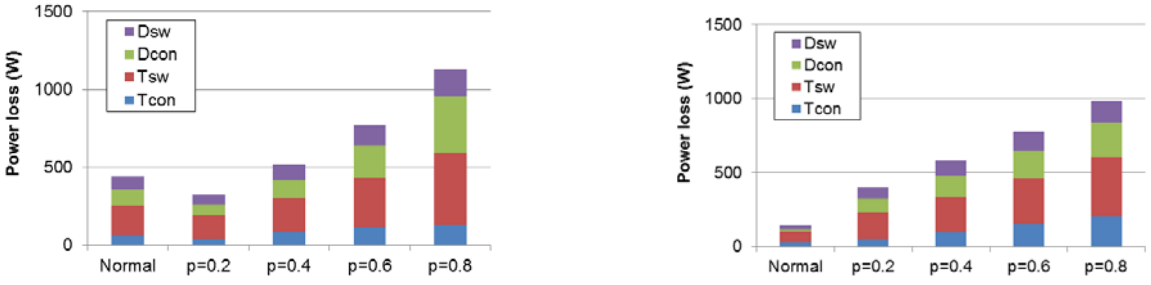

Fig. 11. Power loss distribution at different grid voltage for the rotor-side converter. (a) Rotor speed at1800 rpm; (b) Rotor speed at 1050 rpm.

diode are expressed as current source, the voltage source stand for constant temperature levels, and RC elements are used to signify the thermal impedance.

The thermal impedance from junction to case is modeled as a four-layer Foster RC network, whose values are normally provided by the manufacturer's datasheet. As the Foster structure requires the constant temperature at the terminal, the thermal capacitance of the thermal grease and cooling methods are considered infinite high, which is consequently represented by a controllable voltage source updated by the instantaneous power losses. Meanwhile, the ambient temperature is set to 50 ºC as an indication of the worst case.

Based on the thermal model shown in Fig. 12, the thermal performance of the power device can be simulated again by

PLECS. The simulation of the junction temperature is shown in Fig. 13, where the balanced grid fault to 0.2 pu occurs at the time instant t=4 s.

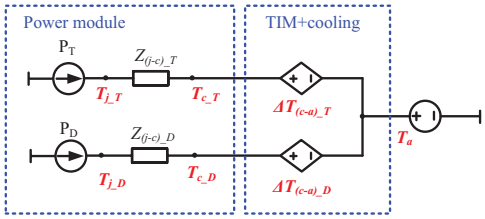

Fig. 12. Thermal model of the power switching device.

Note: TIM stands for Thermal Interface Material.

In case of the rotor speed at 1800 rpm from Fig. 13(a), during the normal operation, the mean junction temperature for the IGBT is higher than the diode, but the junction temperature fluctuation of the diode is higher. If the grid fault happens, the fundamental frequency of the thermal cycling switches from the slip frequency to the rotor speed frequency. Moreover, the switching power device, especially the diode is much more stressed, where the highest junction temperature reach 110 ºC and the junction temperature fluctuation changes from 12.8 ºC to 42.0 ºC.

In the case of the rotor speed at 1050 rpm in Fig. 13(c), the power device is much less stressed in normal operation, which is consistent with the power loss profile shown in the Fig. 11(b). Moreover, the IGBT has a higher mean junction temperature and the junction temperature fluctuation. When the grid fault happens, both the IGBT and the diode become more loaded, and they are more equally heated. The maximum junction temperature fluctuation of the diode changes from 2.3 ºC to 18.4 ºC.

As shown in Fig. 13(b), in which the rotor speed becomes 1500 rpm, the maximum thermal cycling of change from 10.9 ºC in normal operation to 29.3 ºC during the grid faults.

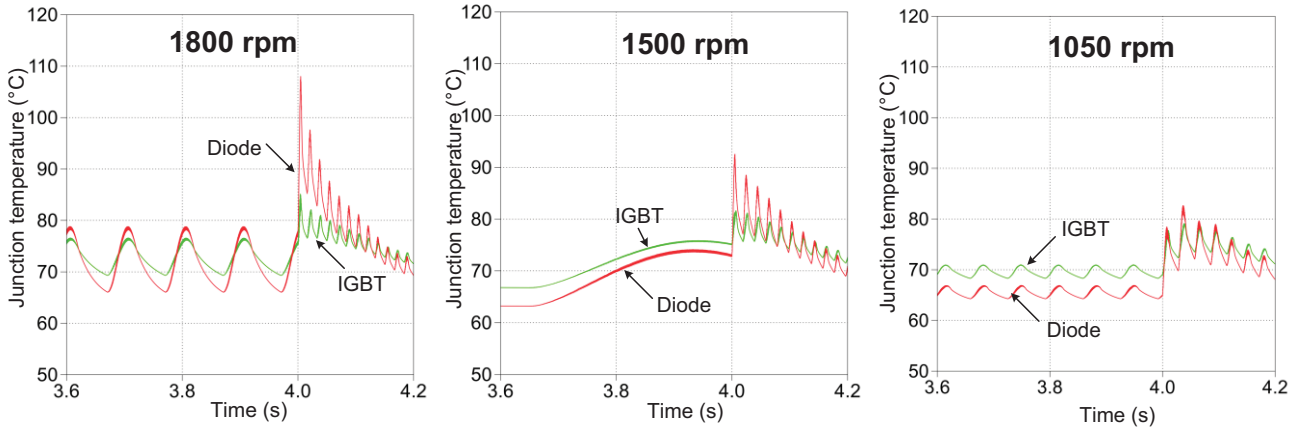

(a) (b) (c)

Fig. 13. Simulation of the junction temperature if the voltage becomes 0.2 pu. (a) Rotor speed at 1800 rpm; (b) Rotor speed at 1500 rpm; (c) Rotor speed at 1050 rpm.

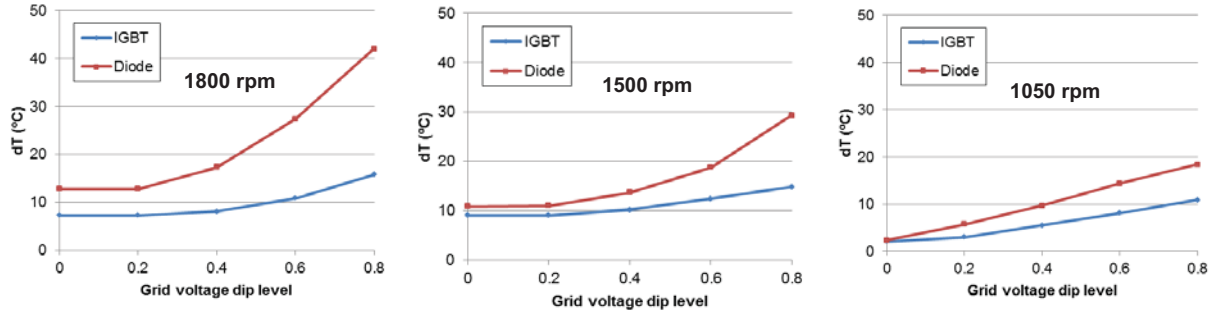

(a) (b) (c)

Fig. 14. Junction temperature fluctuation at different grid voltage dip levels. (a) Rotor speed at 1800 rpm; (b) Rotor speed at 1500 rpm; (c) Rotor speed at 1050 rpm.

In order to evaluate the thermal profile of the power device at different voltage dip levels, Fig. 14 summarizes the junction temperature for the maximum and minimum rotor speeds from the normal operation to the balanced grid fault the voltage dip up to 0.8 pu. At the maximum rotor speed seen from the Fig. 14(a), the shallow voltage dip does not change the value of the junction temperature fluctuation due to the smaller demagnetizing current. If the dip level increases, the junction

temperature fluctuation in the diode has much higher value than the IGBT. Fig. 14(c) shows the situation at the rotor speed 1050 rpm, it is noted that the more voltage dips, the more serious the power device is loaded. As shown in Fig. 14(b), the case that rotor speed becomes 1500 rpm is also investigated.

VI. Conclusion

This paper has studied the impact of rotor current on the stator flux damping time and the rotor terminal voltage for the DFIG in the case of the balanced grid fault.

The safety operation area of the rotor converter by demagnetizing control is theoretically analyzed in terms of the various grid voltage dips and the various rotor speeds. In order to guarantee the same damping time of the stator flux, the simulation also verifies the above safety operation area.

The power loss and thermal behavior are then evaluated for the transient period during balanced grid fault. It is concluded that the serious voltage dip results in higher power losses as well as the junction temperature fluctuation, and may even damage the rotor converter, if the design is not considered carefully.

Appendix

Parameters for a 2 MW DFIG

Ratings: P_n = 2.0 MW, U_s = 563V (phase amplitude), four pole

Turns ratio: $N_s/N_r = 0.369$

Stator resistance: $R_s = 1.688\ \text{m}\Omega$

Stator leakage inductance: $L_s = 0.038$ mH

Rotor resistance: $R_r' = 1.524\ \text{m}\Omega$

Rotor leakage inductance: $L_r' = 0.064$ mH

Magnetizing inductance: $L_m = 2.91$ mH

References

[1] European Commission Climate Action, "*The EU climate and energy package*," Mar. 2007.

[2] F. Blaabjerg, Z. Chen, S. B. Kjaer, "Power electronics as efficient interface in dispersed power generation systems," *IEEE Trans. on Power Electronics*, vol. 19, no. 5, pp. 1184-1194, Sep. 2004.

[3] F. Blaabjerg, K. Ma, D. Zhou, "Power electronics and reliability in renewable energy systems," *in Proc. of ISIE 2012*, pp. 19-30, May. 2012.

[4] S. Yang, A. Bryant, P. Mawby, D. Xiang, L. Ran, P. Tavner, "An industrial-based survey of reliability in power electronic converters," *IEEE Trans. on Industrial Applications*, vol. 47, no. 3, pp. 1441-1451, May. 2011.

[5] H. Polinder, J. A. Ferreira, B. B. Jensen, A. B. Abrahamsen, K. Atallah, R. A. McMahon, "Trends in Wind Turbine Generator Systems," *IEEE Journal of Emerging and Selected Topics in Power Electronics*, vol. 1, no. 3, pp. 174-185, Sep. 2013.

[6] A. Wintrich, U. Nicolai, W. Tursky, T. Reimann, "*Application manual power semiconductors*," Semikron international GmbH, Nuremburg, 2011.

[7] ZVEL, Handbook for robustness validation of automotive electrical/electronic modules, Jun. 2008.

[8] F. Richardeau, T. T. L. Pham, "Reliability calculation of multilevel converters: theory and applications," *IEEE Trans. on Industrial Electronics*, vol. 60, no. 10, pp. 4225-4233, Oct. 2013.

[9] H. Behjati, A. Davoudi, "Reliability analysis framework for structural redundancy in power semiconductors," *IEEE Trans. on Industrial Electronics*, vol. 60, no. 10, pp. 4376-4386, Oct. 2013.

[10] ABB Application Note, Load-cycling capability of HiPaks, 2004

[11] D. Xiang, L. Ran, P. J. Tavner, S. Yang, "Control of a doubly fed induction generator in a wind turbine during grid fault ride-through,", *IEEE Trans. on Energy Conversion*, vol. 21, no. 3, pp. 652-662, Sep. 2006.

[12] J. Lopez, E. Gubia, E. Olea, J. Ruiz, L. Marroyo, "Ride through of wind turbines with doubly fed induction generator under symmetrical voltage dips," *IEEE Trans. on Industrial Electronics*, vol. 56, no. 10, pp. 4246-4254, Oct. 2009.

[13] W. Chen, D. Xu, M. Chen, F. Blaabjerg, "Comparison of current control strategies for DFIG under symmetrical grid voltage dips," *in Proc. of IECON 2013*, pp. 1540-1545, Nov. 2013.

[14] J. Liang, W. Qiao, R.G. Harley, "Feed-forward transient current control for low voltage ride-through enhancement of DFIG wind turbines", *IEEE Trans. on Energy Conversion*, vol. 25, no. 3, pp. 836-843, Sep. 2010.

[15] F. K. A. Lima, A. Luna, P. Rodriguez, E. H. Watanabe, F. Blaabjerg, "Rotor voltage dynamics in the doubly fed induction generator during grid faults", *IEEE Trans. on Power Electronics*, vol. 25, no. 1, pp. 118-130, Jan. 2010.

[16] R. Cardenas, R. Pena, S. Alepuz, G. Asher, "Overview of control systems for the operation of DFIGs in wind energy applications," *IEEE Trans. on Industrial Electronics*, vol. 60, no. 7, pp. 2776-2798, July 2013.

[17] S. Xiao, G. Yang, H. Zhou, H. Geng, "An LVRT control strategy based on flux linkage tracking for DFIG-based WECS," *IEEE Trans. on Industrial Electronics*, vol. 60, no. 7, pp. 2820-2832, July 2013.

[18] K. Ma, F. Blaabjerg, M. Liserre, "Operation and thermal loading of three-neutral-point-clamped wind power converter under various grid faults," *in Proc. of ECCE 2012*, pp. 2410-2418, 2012.

[19] D. Zhou, F. Blaabjerg, M. Lau, M. Tonnes, "Thermal analysis of two-level wind power converter under symmetrical grid fault," *in Proc. of IECON 2013*, pp. 1902-1907, Nov. 2013.

[20] E.ON-Netz. *Requirements for offshore grid connections*, Apr. 2008.

[21] M. Tsili, S. Papathanassiou, "A review of grid code technical requirements for wind farms," *IET on Renewable Power Generation*, vol. 3, no. 3, pp. 308-332, Sep. 2009.

[22] G. Abad, J. Lopez, M. Rodriguez, L. Marroyo, G. Iwanski, *Doubly fed induction machine-modeling and control for wind energy generation.* Piscataway, NJ: IEEE Press, 2011, pp. 265-302.

[23] D. Zhou, F. Blaabjerg, M. Lau, M. Tonnes, "Thermal analysis of multi-MW two-level wind power converter," *in Proc. of IECON 2012*, pp.5862-5868, Oct. 2012.

[24] D. Zhou, F. Blaabjerg, M. Lau, M. Tonnes, "Thermal cycling overview of multi-metawatt two-level wind power converter at full grid code operation," *IEEJ Journal of Industry Applications*, vol. 2, no. 4, pp. 173-182, Jul. 2013.

[25] User manual of PLECS blockset version 3.2.7 March 2011. (Available: http://www.plexim.com/files/plecsmanual.pdf